

University of Groningen

Recombinant myelin oligodendrocyte glycoprotein quality modifies evolution of experimental autoimmune encephalitis in macaques

Stimmer, Lev; Confais, Joachim; Jong, Anke't; Veth, Jennifer; Fovet, Claire-Maëlle; Horellou, Philippe; Massonneau, Julie; Perrin, Audrey; Miotello, Guylaine; Avazeri, Emilie

Published in:
Laboratory Investigation

DOI:
[10.1038/s41374-021-00646-x](https://doi.org/10.1038/s41374-021-00646-x)

IMPORTANT NOTE: You are advised to consult the publisher's version (publisher's PDF) if you wish to cite from it. Please check the document version below.

Document Version
Publisher's PDF, also known as Version of record

Publication date:
2021

[Link to publication in University of Groningen/UMCG research database](#)

Citation for published version (APA):

Stimmer, L., Confais, J., Jong, A., Veth, J., Fovet, C-M., Horellou, P., Massonneau, J., Perrin, A., Miotello, G., Avazeri, E., Hart, B., Deiva, K., Le Grand, R., Armengaud, J., Bajramovic, J. J., Contamin, H., & Serguera, C. (2021). Recombinant myelin oligodendrocyte glycoprotein quality modifies evolution of experimental autoimmune encephalitis in macaques. *Laboratory Investigation*, *101*(11), 1513-1522. <https://doi.org/10.1038/s41374-021-00646-x>

Copyright

Other than for strictly personal use, it is not permitted to download or to forward/distribute the text or part of it without the consent of the author(s) and/or copyright holder(s), unless the work is under an open content license (like Creative Commons).

The publication may also be distributed here under the terms of Article 25fa of the Dutch Copyright Act, indicated by the "Taverne" license. More information can be found on the University of Groningen website: <https://www.rug.nl/library/open-access/self-archiving-pure/taverne-amendment>.

Take-down policy







If you believe that this document breaches copyright please contact us providing details, and we will remove access to the work immediately and investigate your claim.

Downloaded from the University of Groningen/UMCG research database (Pure): <http://www.rug.nl/research/portal>. For technical reasons the number of authors shown on this cover page is limited to 10 maximum.

TECHNICAL REPORT



Recombinant myelin oligodendrocyte glycoprotein quality modifies evolution of experimental autoimmune encephalitis in macaques

Lev Stimmer^{1,2}, Joachim Confais³, Anke't Jong⁴, Jennifer Veth⁴, Claire-Maëlle Fovet^{1,5}, Philippe Horellou⁵, Julie Massonneau¹, Audrey Perrin¹, Guylaine Miotello⁶, Emilie Avazeri⁶, Bert't Hart⁷, Kumaran Deiva^{5,8}, Roger Le Grand⁵, Jean Armengaud⁶, Jeffrey J. Bajramovic⁴, Hugues Contamin³ and Ché Serguera^{1,2,9}

© The Author(s), under exclusive licence to United States and Canadian Academy of Pathology 2021

Experimental autoimmune encephalitis (EAE) is a well-recognized model for the study of human acquired demyelinating diseases (ADD), a group of inflammatory disorders of the central nervous system (CNS) characterized by inflammation, myelin loss, and neurological impairment of variable severity. In rodents, EAE is typically induced by active immunization with a combination of myelin-derived antigen and a strong adjuvant as complete Freund's adjuvant (CFA), containing components of the mycobacterial wall, while myelin antigen alone or associated with other bacterial components, as lipopolysaccharides (LPS), often fails to induce EAE. In contrast to this, EAE can be efficiently induced in non-human primates by immunization with the recombinant human myelin oligodendrocyte glycoprotein (rhMOG), produced in *Escherichia coli* (*E. coli*), purified and formulated with incomplete Freund's adjuvant (IFA), which lacks bacterial elements. Here, we provide evidence indicating how trace amounts of bacterial contaminants within rhMOG may influence the course and severity of EAE in the cynomolgus macaque immunized with rhMOG/IFA. The residual amount of *E. coli* contaminants, as detected with mass spectrometry within rhMOG protein stocks, were found to significantly modulate the severity of clinical, radiological, and histologic hallmarks of EAE in macaques. Indeed, animals receiving the purest rhMOG showed milder disease severity, increased numbers of remissions, and reduced brain damage. Histologically, these animals presented a wider diversity of lesion types, including changes in normal-appearing white matter and prephagocytic lesions. Non-human primates EAE model with milder histologic lesions reflect more accurately ADD and permits to study of the pathogenesis of disease initiation and progression.

Laboratory Investigation (2021) 101:1513–1522; <https://doi.org/10.1038/s41374-021-00646-x>

INTRODUCTION

Experimental autoimmune encephalitis (EAE) is a neurological affection induced in animals mimicking acquired demyelinating diseases (ADD), a group of inflammatory diseases of the central nervous system (CNS) characterized by inflammation, myelin loss, and neurological impairment of variable severity¹. EAE is typically induced in rodents by active immunization with myelin-derived antigens emulsified with strong adjuvants as complete Freund's adjuvant (CFA), which contains mycobacterial membrane components, and/or *Bordetella pertussis* toxin^{2,3}. These adjuvants induce a powerful inflammatory response associated with blood-brain-barrier (BBB) permeability^{4,5}. Indeed, during the process of immunization, the adjuvant bacterial antigens relay "danger" signals in phagocytic antigen-presenting cells (APC) via activation of innate pattern recognition receptors (PRR) as Toll-like receptors

(TLR) and NOD-like receptors (NLR), inducing archetypical activation of naïve CD4+ T cells into myelin-directed T helper type 1 (Th1) autoreactive T cells⁶. To intend shifting the type of anti-myelin autoimmune response, novel schemes of immunization have been explored replacing CFA or *B. pertussis* toxin with other adjuvants^{7,8}. It has been proposed that certain bacterial components, such as bacterial DNA or lipopolysaccharides (LPS), can replace CFA in mediating EAE^{9,10}. Other bacterial components such as muramyl-dipeptide and mycobacterial glycolipid—6, 6'-trehalose-dimycolate, have also been efficiently used to induce EAE in mice^{11–14}. Modulation of the clinical course of EAE has been observed by altering the adjuvant. Administration of MOG_{92–106} peptide in CFA to ASW mice resulted in a primary progressive (PP) disease course, whereas the same scheme with *B. pertussis*, resulted in a secondary progressive (SP) EAE¹⁵. In fact, in ASW

¹Commissariat à l'Énergie Atomique (CEA), Institut de Biologie François Jacob, Molecular Imaging Research Center (MIRCen), Fontenay-aux-Roses, France. ²INSERM, UMR 1127, Paris Brain & Spine Institute (ICM), Paris, France. ³Cynbiose, Marcy-l'étoile, France. ⁴Alternatives Unit, Biomedical Primate Research Centre (BPRC), Rijswijk, the Netherlands. ⁵Université Paris-Sud, CEA, Inserm UMR 1184 and Institut de biologie François Jacob, Infectious Diseases Models for Innovative Therapies (IDMIT), Fontenay-aux-Roses, France. ⁶Département Médicaments et Technologie pour la Santé (DMTS), Université Paris-Saclay, CEA, INRAE, SPI, Bagnols-sur-Cèze, France. ⁷Department Anatomy and Neuroscience, Amsterdam University Medical Center (VUMC), Amsterdam, Netherlands and University of Groningen, Department Biomedical Sciences of Cells and Systems, University Medical Center Groningen, Groningen, the Netherlands. ⁸AP-HP, Hôpitaux Universitaires Paris Saclay, Department of Pediatric Neurology, National Reference Center for Rare Inflammatory and Auto-immune Brain and Spinal Diseases, Paris, France. ⁹Asfalia Biologics, Paris Brain & Spine Institute (ICM), Paris, France. [✉]email: lev.stimmer@inserm.fr

Received: 14 March 2021 Revised: 11 July 2021 Accepted: 16 July 2021
Published online: 10 August 2021

mice, the supplementation with *B. pertussis* appeared to be protective¹⁶.

Interestingly and different from immunologically immature SPF rodents, EAE can be induced in different species of non-human primates (NHP) using recombinant human myelin oligodendrocyte glycoprotein (rhMOG) emulsified in incomplete Freund's adjuvant (IFA), lacking mycobacterial extract. In these animals, EAE is of variable severity and can be monophasic or relapsing, affecting the brain, and less frequently, the spinal cord and the optic nerve¹⁷. This indicates that the development of EAE in NHP immunized with rhMOG/IFA, relies on recalled memory T lymphocytes rather than newly activated naïve T cells¹⁸.

Moreover, in the absence of the polarizing effect of CFA and *pertussis* toxin these NHP models reflect more closely the wide range of autoimmune responses observed in ADD subsets^{17,19}.

In the present study, we describe the variable severity of EAE in the cynomolgus macaque species depending on the use of purified batches of rhMOG protein, either obtained from an industrial provider or prepared in our laboratory. Variable amounts of *Escherichia coli* (*E. coli*) contaminants between the batches, as evaluated with mass spectrometry, appeared to be a prominent factor influencing the severity of EAE, the imaging aspect of lesions as well as their histologic appearance.

MATERIALS AND METHODS

Study origin

The present study compares the course of EAE in *Macaca fascicularis* performed in two distant French facilities, through immune sensitization with rhMOG. When we first analyzed the clinical outcome of the two protocols, we were surprised by the milder form of EAE observed in Cynbiose (Marcy l'Etoile, France) animals as compared to that currently modeled at MIRCen (Fontenay aux Roses, France)^{17,20}. We reasoned that several factors could explain such difference: (1) misrouting of intradermal injection of rhMOG may preclude EAE outcome, but this procedure was executed in both places by the same experienced surgeon. (2) The intestinal flora of animals can modulate the immune outcome of rhMOG immunization²¹. The main factors shaping the microbiome would be the origin of animals, the sanitary procedures and vaccinations, the daily follow-up, and the diet, but these variables were all equivalent in both facilities (see Supplementary Table 1). We then low-ranked these occurrences as causing EAE variations. (3) Sex and age may influence immunity; while the number of males and females was not different between the two cohorts (Fisher's exact test $p = 0.6641$), MIRCen's animals were older than that of Cynbiose (unpaired t test, $p < 0.0001$) (Supplementary Table 2). A Pearson r correlation between "age" and the other variables (onset, days ill, remissions/relapses (R/R), # of lesions, lesions area, and levels of anti-MOG IgG), indicated no correlation, but in one case, between age and remissions/relapses ($p = 0.0321$). However, within each group, age and R/R were not correlated (MIRCen: $p = 0.56$; Cynbiose $p = 0.96$). As the Cynbiose group includes the widest range of ages and the highest number of animals with R/R, an absence of correlation between age and R/R in this group, points at an artifact when computing age and R/R in the 18 macaques involved in the study. Moreover, if "age" would influence the disease evolution, it would covariate with most of the variables, which is not the case. We then considered that the age of the animals was not the factor influencing EAE evolution. (4) We then alleged that the quality of the batches of rhMOG used in either protocol could influence the autoimmune response. Weighing the aforementioned arguments together with the fact that each batch of rhMOG contained a significantly different amount of bacterial contaminant, made us postulate that the quality of rhMOG was the most likely factor influencing EAE outcomes in our experiments.

Animals and study design

In this study, we compared the clinical and histopathological outcome in two groups of adult macaques immunized with two different batches of rhMOG (rhMOG-1 and rhMOG-2), used to immunize animals in two separate laboratories. The study includes a total of 18 adult cynomolgus macaques (*Macaca fascicularis*) immunized with rhMOG/IFA. One group includes ten macaques (5 males and 5 females) immunized at the MIRCen institute (CEA, Fontenay aux Roses, France), and a second group includes 8

Table 1. Clinical, MRI, and histopathologic parameters of EAE and brain lesions.

		MOG1	MOG2
Clinical observations	Number of animals	10	8
	Age (years) ^a	8.14	4.79
	Sex	5♂/5♀	3♂/5♀
	Onset (dpi) ^a	40.8	53
	Days ill ^a	5.2	19.8
	Clinical grade ^a	3.5	2.9
	Number of remissions ^a	0.1	0.9
	Anti-MOG IgG (AU) ^a	1014381.1	29713.3
MRI	Lesion number ^a	2.8	3.6
	Lesion area (cm ²) ^a	62.6	29.3
Histopathologic evaluation	Cumulative severity score ^a	13.5	7.9
	Microglia activation ^a	2.8	2.1
	Astrocytic activation ^a	2.6	1.9
	IgG deposition ^a	2.5	1.9
	Complement activation ^a	1.6	2.1
	Cumulative lesion type frequency		
	Lesion type 1	21 (75.0%)	5 (33.3%)
	Lesion type 2	3 (10.7%)	5 (33.3%)
Lesion type 3	4 (14.3%)	1 (6.7%)	
Lesion type 4	0 (0.0%)	4 (26.7%)	

^aMean value of the group; the cumulative lesion frequency reflects the sum of observed lesions for each lesion type in animals immunized with MOG1 or MOG2. Lesions, type 1: confluent demyelination; type 2: perivascular mononuclear infiltration; type 3: myelin vacuolation; type 4: normal-appearing white matter.

animals (3 males and 5 females) immunized at the Cynbiose facility (Marcy l'étoile, France) (Table 1 and Supplementary Table 2). Both laboratories used the exact same procedures for animal immunization, clinical observation, and sample collection but employed rhMOG of different origins.

Immunization protocols, clinical observations, cerebrospinal fluid (CSF), and blood collection methods were described in our previous publication²⁰. Briefly, three to 10-year-old cynomolgus macaques of either sex were purpose-bred animals imported from a licensed primate-breeding center in Mauritius (Cynologics Ltd, Port Louis, Mauritius). Following European directive 2010/63/UE and French regulations, the project at MIRCen was performed in an agreed user establishment (agreement number C 92-032-02), with institutional permission obtained from the French Ministry of Agriculture after evaluation by an ethical committee (2015081710528804v1). At Cynbiose (agreement number N°C 69 127 0505), the project was approved by the ethical committee of VetAgro Sup (2016072117544328) under file number 1417v2. All procedures were performed in compliance with CEA's and Cynbiose's animal welfare structure under veterinary care at all times (Supplementary Table 1). Monkeys remained under veterinary care during both studies. Venous blood samples were collected every week, starting before the first immunization with rhMOG/IFA and until the end of experimentation, as well as at EAE onset and before euthanasia, with a maximum volume of up to 15% of the total blood volume per animal per month (26 ml). Blood was centrifuged and plasma was stored at -80°C . Before sample collections, immunization, or Magnetic Resonance Imaging (MRI), animals were sedated with ketamine hydrochloride (Imalgene, 15 mg/kg, intramuscular injection) and xylazine (Rompun 2% 0.5 mg/kg, intramuscular injection).

Anesthesia was maintained during MRI acquisition with propofol (Propovet, 10 mg/kg/h, intravenous infusion on the external saphenous vein).

Production of rhMOG and animal's immunization

The rhMOG used to immunize the MIRCen group of macaques (rhMOG-1) was produced at BPRC (Rijswijk, The Netherlands), as described earlier^{20,22}. Briefly, the amino acids 1-125 of the human MOG fused with an N-terminal His-Tag was produced in *E. coli* and was purified using an FPLC column with a resin that bound this specific tag. The protein was eluted, and its concentration and purity were checked by using a Nanodrop, a BCA protein assay (A53225, Thermo Fisher), and an ELISA; the absence of contaminant proteins was assessed through Western blot as described^{20,22}. The rhMOG-2 used at Cynbiose, consisted of the same fragments 1-125 of human MOG with an N-term His-Tag. It was also produced in *E. coli* using a pET28a plasmid leading to purity $\geq 90\%$ and with a level of endotoxin < 1 eu/ μ g (GeneCust, 6 rue Dominique Lang, L-3505 Dudelange-Luxembourg) as reported by the provider.

Animals were immunized every 4 weeks with 300 μ g of rhMOG (1 mg/ml) in IFA (Sigma-Aldrich, St. Quentin Fallavier France) until disease onset, in the dorsal skin by 6 intradermal injections of 100 μ l (50 μ g rhMOG per injection site). The immunogen preparations for immunization of all cynomolgus macaques were prepared by dissolving 300 μ g rhMOG in 300 μ l PBS, emulsified with an equal volume of IFA (Sigma-Aldrich, St. Quentin Fallavier, France). Ten macaques were immunized in the MIRCen NHP research facility (Fontenay-aux-Roses, France) with rhMOG-1 protein (MOG1). In addition, 8 macaques were immunized in the Cynbiose research facility using the same procedure, with direct support from MIRCen staff to perform the intradermal injection, using rhMOG-2 protein (MOG2).

Clinical observations

Monkeys were observed daily throughout our experiments. Clinical scores were assessed using a semi-quantitative functional scale with the severity of disease implying closer endpoints of experiments²⁰. Macaques were observed double-blinded daily from immunization until the end of the experiment; they were scored daily for EAE outcome directly by the experimenter or through webcam surveillance, using a semi-quantitative functional scale. Endpoints are based on the evaluation of disease gravity, with increased severity shortening the time of the experiment, ultimately ending with animal euthanasia. Briefly, disease severity was graded from 0 (healthy), grade 0.5 (loss of appetite, vomiting), grade 1 (apathy), grade 2 (ataxia, sensory loss and/or visual problems), grade 2.5 (hemiparesis or paraparesis), grade 3 (hemiplegia or paraplegia), grade 4 (quadriplegia), to grade 5 (protraction), all corresponding to classical neurological signs and symptoms conducing to ADS diagnosis (Supplementary Table 3).

Anti-MOG IgG antibodies

The concentration of anti-rhMOG IgG in plasma from cynomolgus monkeys was assessed by ELISA in 96-well plates. Flat bottom plastic plates (Costar 3595, Corning) were coated with rhMOG (5 μ g/ml PBS1x) overnight at 4 °C. After washing and blocking with PBS/1% BSA, the wells were incubated with 1:200 or 1:2000 diluted plasma samples. Bound antibodies were detected with alkaline phosphate-labeled goat-anti-human IgG (1:1000, 4H11305, Invitrogen Life Technologies, Bleiswijk, Netherlands). Conjugate binding was quantified with SIGMAFAST p-nitrophenyl phosphate (Sigma, St. Quentin Fallavier France). Measured optical density was converted to arbitrary units (AU) using a concentration curve of the same positive control as reference.

Magnetic resonance imaging (MRI)

For macaques followed at the MIRCen facility, MRI acquisitions were performed on a horizontal 7T Agilent scanner (Palo Alto, CA, USA), using a surface coil for transmission and reception (RAPID Biomedical GmbH, Rimpf, Germany). T2-weighted images were acquired using a high-resolution 2D fast spin-echo sequence. Lesion segmentation was performed on the T2-weighted images. During scanning, animals were anesthetized and maintained in a dedicated stereotaxic frame. The respiratory rate was monitored (SA Instruments Inc., Stony Brook, NY, USA) and body temperature was maintained at 37 °C using a heated waterbed. Lesions were manually delineated slice-by-slice by a single operator to measure their volume.

For macaques monitored at Cynbiose, MRI was performed at the CERMEP-PRIMAGE imaging facility, using a 3 T MRI (Siemens MAGNETOM Prisma, Siemens, Erlangen, Germany). The animals were maintained under fixed IV anesthesia and their vitals were monitored. Their body temperature was kept at 37 °C using a heating blanket, and their head was kept straight and stable in a soft frame tightened around their skull. The structural imaging sequence was as follows: coronal sections acquired via a T1-weighted 3D MPR sequence, a T2-weighted 3D SPC sequence, and a FLAIR 3D SPC sequence. The lesions were delineated using the T2-weighted images and verified with the two other sequences, using the MITK 3M3 (v1.1.0.; developed by Mint Medical and the German Cancer Research Center). Lesion sizes were calculated using the `fsstats-V` function of the FMRIB Software Library (v5.0; FSL, Oxford, UK).

Histology and immunohistochemistry

All histologic procedures were performed and analyzed at MIRCen by Dr. Lev Stimmer. The evaluation of the slides was performed in a blinded manner.

Tissue preparation. Brains were sampled after intracardiac perfusion with PBS and 4% PFA and were postfixed by overnight immersion in 4% PFA and then transferred to PBS and embedded in paraffin. Brains were sliced in 12–15 slices of 4 mm thickness using a dedicated brain dissection matrix. Slices were included in standard super cassettes (75 × 52 × 17 mm) using internal standard operating procedures. For the histochemical analyses 3–5 μ m-thick paraffin sections were cut, deparaffinized, and stained with the following histochemical stains: Hematoxylin/Eosin (HE; evaluation of inflammation), Luxol fast blue/Periodic Acid Schiff (LFB/PAS; evaluation of demyelination) according to the institute standard operating procedures. Furthermore, immunohistochemistry was used to investigate microglia/macrophages and astrocyte activation, T cell infiltration, and intracerebral IgG and complement protein C1q distribution. Briefly, paraffin wax-embedded tissues were dewaxed in xylene and hydrated through graded alcohols. Endogenous peroxidase activity was suppressed by 3% H₂O₂ in PBS. Subsequently, sections were incubated with anti-CD3 (A0452, Dako, Les Ulis, France; dilution 1/100), anti-Iba 1 (Fujifilm Wako Chemicals U.S.A. Corp; dilution 1/500), anti-GFAP (Z0334, Dako, Les Ulis, France; dilution 1/1000), anti-IgG (anti-human IgG (gamma chain), 1/100, SAB3701291, Sigma-Aldrich, Saint-Louis, MI, USA), or anti-Human C1q, (1/100, A0136, Dako, Les Ulis, France). The biotinylated rabbit-anti-goat or goat-anti-rabbit antibodies were used as secondary antibodies, for 30 min at room temperature, followed by the avidin-biotin-peroxidase complex (Vectastain Elite ABC Kit, Vector Laboratories, PK 6100; Burlingame, CA, USA). Positive antigen-antibody reactions were visualized by incubation with 3,3'-diaminobenzidine-tetrahydrochloride (DAB)-H₂O₂ in 0.1 M imidazole, pH 7.1 for 5 min, followed by slight counterstaining with hematoxylin. Brain and spinal cord lesions were scored according to their overall severity, number, size, and morphological characteristics as well as according to the intralesional myelin loss. Identified brain lesions were classified in four lesion types: the lesion type 1—myelin destruction, with variable necrosis and hemorrhage, lesion type 2—perivascular infiltration with minimal visible neuropil changes and microglial and astrocytic activation, lesion type 3—myelin vacuolation with microglial and astrocytic activation and with minimal cellular infiltrate, lesion type 4—normal-appearing white matter (HE) and microglial and astrocytic activation. Furthermore, the severity of intralesional hemorrhage, necrosis, and myelin vacuolation was graded using three severity grades scale (i.e., mild, moderate, marked). In addition, the severity of inflammatory infiltration including CD3 positive lymphocytes, microglia/macrophages, and neutrophils, was evaluated in the perivascular space and in the neuropil using the same grading scale. The cumulative severity score was calculated as the sum of the severity grades of all the above-named parameters. The same grading scale was used for evaluation of the severity of microglia/macrophagic and astrocytic activation as well as of the severity of the immunoglobulin G deposition (IgG) and of the complement protein C1q expression.

Proteomics analysis of rhMOG-1 and rhMOG-2

A total of 10 μ g of each protein preparation was diluted with Novex NuPAGE 4X LDS Sample Buffer (Invitrogen) supplemented with β -mercaptoethanol, and milliQ water, resulting in samples containing 10 μ g in a final volume of 30 μ l of LDS 1X. Two technical duplicates were performed for each protein preparation, resulting in four samples that were treated to generate trypsin peptides as previously described²³.

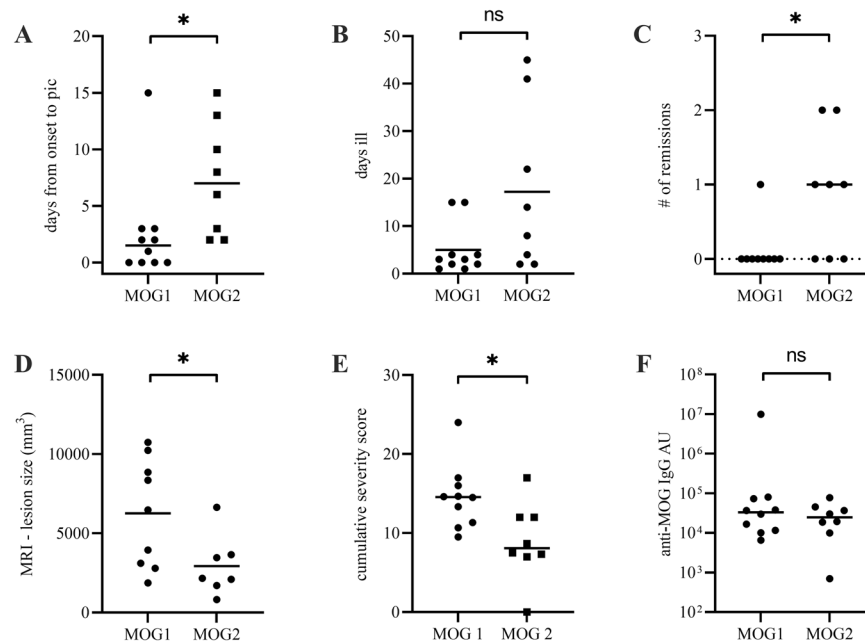


Fig. 1 The most relevant clinical, imaging, and histologic parameters. **A** Mean time from onset to pic of EAE in days post-onset. **B** Total sum of days with clinical signs of EAE. **C** Number of remissions of EAE observed in each animal. **D** Area of brain lesions measured with MRI before euthanasia. **E** Cumulative severity score of observed histopathologic lesions. **F** Levels of anti-MOG IgG in plasma at euthanasia. MOG1 refers to animals immunized with rhMOG1 and MOG2 to animals immunized with rhMOG2. * $P \leq 0.05$; ns not significant. Horizontal lines: median values of the group.

Briefly, samples were subjected to a short (5 min) electrophoretic migration on NuPAGE 4–12% Bis-Tris gel (Invitrogen) performed at 200 V in MES/SDS 1X running buffer (Invitrogen). The polyacrylamide bands containing the whole protein content of each sample were proteolyzed with gold mass spectrometry grade trypsin (Promega) in the presence of 0.01% ProteaseMAX detergent (Promega). A fraction of the resulting peptides (10 μ L out of 55 μ L) were analyzed in a data-dependent mode with an ESI-Q Exactive HF mass spectrometer (Thermo) coupled to an Ultimate 3000 nanoLC System (Thermo) operated as previously reported²⁴. Peptides were resolved onto a reverse-phase Acclaim PepMap 100 C18 column (3 μ m, 100 Å, 75 μ m internal diameter, 500 mm) with a 60 min gradient of acetonitrile in presence of 0.1% formic acid. The mass spectrometer was operated with Top20 standard parameters and a dynamic exclusion of 10 s. MS/MS spectra were searched using the Mascot Daemon software (Matrix Science) against a database comprising the rhMOG sequence and *E. coli* annotated protein sequences. Peptide-to-MS/MS spectrum matching with a p -value below 0.05 was selected and assigned to a unique peptide sequence following the parsimony principle. A protein was considered valid when at least two different peptides were detected. The false-positive rate for protein identification was estimated by a search with a reverse decoy database to be below 1% with these parameters. Proteins were quantified based on their spectral counts and their ratio among all proteins was estimated based on their percentage of normalized spectral abundance factor (NSAF) calculated as described²⁵.

Innate immune stimulatory activity of rhMOG

The two batches of rhMOG were screened for the presence of innate immune receptor ligands in bioassays. We used the THP-1 monocyte cell line and HEK293 cells that were stably transfected with the luciferase gene as a reporter under the control of an NF- κ B-dependent promoter. As the THP-1 cells express a multitude of innate immune receptors, this bioassay is not specific but provides a rather crude overview. Endogenous expression levels of different innate immune receptors in HEK293 cells are very low and were therefore used as specific reporter cells for individual innate immune receptors. Therefore, they were transfected with different Toll-like receptors (TLR) or with the nucleotide oligomerization domain receptor 2 (NOD2), as described earlier²². As a positive control for non-TLR induced, NF- κ B mediated activation we used exposure to TNF α at 25 ng/ml (Preprotech, London, UK). Ligand specific positive controls were PAM3CSK at 1 μ g/ml for the TLR2 bioassay, ULP5 at 10 μ g/ml for the TLR4 bioassay, Flagellin at 1 μ g/ml for the TLR5 bioassay, and Muramyl dipeptide

(MDP) at 10 μ g/ml for the NOD2 bioassay. All ligands were purchased from InvivoGen (San Diego, CA), except LPS, which was obtained from Sigma-Aldrich.

Statistical analysis

Statistical analyses and graphical representations were done using Prism 8 (GraphPad Software, Inc). One- and two-sided one-way ANOVA test with Tukey's multiple comparisons was used to compare three groups or more values. Unpaired t test was used to compare two groups of values. Pearson correlation coefficient was used to measure the linear association between age and the other variables listed in Supplementary Table 2.

RESULTS

Clinical evolution of EAE in macaques immunized with rhMOG

In this study, we compare the clinical characteristics of EAE between two groups of adult cynomolgus macaques immunized with rhMOG/IFA. In one group, ten macaques were immunized with rhMOG produced at BPRC (MOG1), while in the second, eight macaques were immunized with rhMOG purchased from GeneCust (MOG2). All animals of either group developed a classical EAE with common signs of encephalitis and multifocal neurological deficits (Table 1, Supplementary Table 4). However, several clinical parameters indicated that diseases evolved differently in either group of animals. For instance, macaques of group MOG1 tended to present EAE onset earlier than that of the group MOG2, at a median time of 31.5- versus 39.5-days post-immunization (dpi) respectively (Supplementary Fig. 1). In addition, animals of the group MOG1 suffered a much faster progression from first signs to the peak of disease, while in animals of group MOG2, EAE appeared to be more progressive (Fig. 1A ($p = 0.02$) and B ($p = 0.05$)); animals of group MOG2 also had significantly more remissions than animals of group MOG1 (Fig. 1C ($p = 0.04$)). In all animals but one (M2-8), EAE onset was confirmed by anomalous MRI with multiple hyperintense signals spread in different areas of the brain and the spinal cord. In both groups, the lesions detected at MRI had a similar diffuse aspect with poorly defined borders as described before²⁶. Then, even though animals

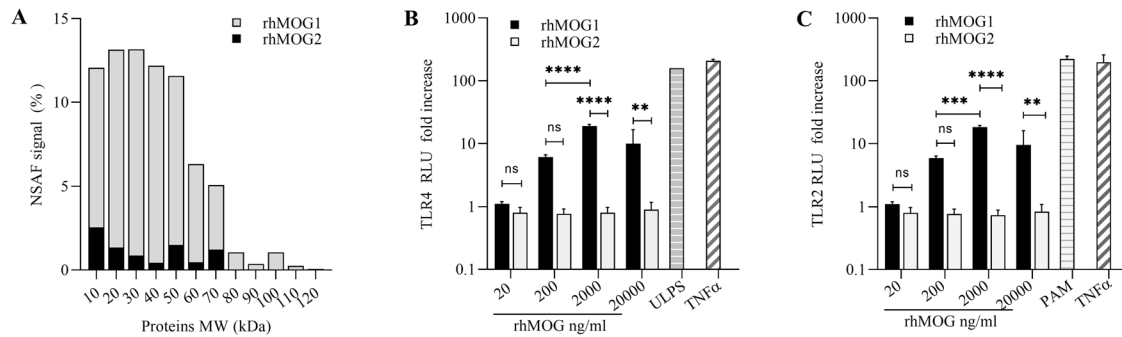


Fig. 2 Proteomic detection of contaminating proteins in rhMOG batches, and their stimulating effect on innate immunity. **A** The spectral count of *E. coli* proteins detected in the batches of rhMOG-1 and rhMOG-2 were quantified and normalized according to their molecular weight and expressed as normalized spectral abundance factor (NSAF). Host cell proteins from *E. coli* of all ranges of molecular weights were much more abundant in rhMOG-1 than in rhMOG-2. **B**, **C** TLR2 and TLR4 stimulatory activity of rhMOG-1 and rhMOG-2 as measured in HEK293 cells transfected with TLR2 or TLR4. Positive controls include stimulation with specific ligands of TLR2 (PAM3CSK (PAM) at 1 μ g/ml or TNF α at 25 ng/ml) and TLR4 (ULPS at 10 μ g/ml or TNF α at 25 ng/ml). Statistics, Two-way ANOVA with Tukey multiple comparisons test. *P* value summary, **P* \leq 0.05; ***P* \leq 0.01; ****P* \leq 0.001, *****P* \leq 0.0001.

of both groups displayed an equivalent number of brain lesions at the last MRI before euthanasia, the size of brain lesions in animals of group MOG1 was significantly larger than that detected in animals of group MOG2 (Fig. 1D ($p = 0.04$)). Finally, although animals of group MOG1 had an increased cumulative severity score (see below) as compared to animals of group MOG2 (Fig. 1E ($p = 0.02$)), and despite the many differences during clinical EAE, both groups of macaques had an equivalent increased amount of anti-MOG IgG (Fig. 1F ($p = 0.34$)), and presented no difference in the severity of EAE at euthanasia (Supplementary Table 2).

These observations indicate that animals of group MOG1 developed a more acute EAE than that observed in animals of group MOG2, in which the disease evolved more progressively.

Analysis of bacterial contaminants in rhMOG batches

For immunizations, we used the adjuvant IFA, a mineral oil emulsion lacking bacterial components; this mixture associated with rhMOG, typically produces milder forms of EAE in marmosets as compared to rhMOG administered in CFA, which contains mycobacterial extracts²⁰. Thus, after weighing the possible implication of several factors in modifying the course of EAE (see "Study origin" in Materials and methods), we hypothesized that the quality of the recombinant MOG could explain the observed clinical variations described above. The degree of contamination of both rhMOG preparations with bacterial factors was assessed by quantifying the presence of *E. coli* host cell proteins (HCP) contaminants in the batches of purified rhMOG. Thus, we analyzed twice each lot of rhMOG-1 and rhMOG-2 with shotgun proteomics. The tandem mass spectrometry highly sensitive approach detected 779 proteins from *E. coli*, among which 577 were retrieved with at least two peptide sequences. Among these 577 well-confirmed proteins, more than 80% were present in rhMOG-1 but only 14% in rhMOG-2 (Supplementary Fig. 2A). Moreover, from 96 *E. coli* proteins detected with an abundance above 0.2% of Normalized Spectral Abundance Factor (NSAF), more than 90% were detected in rhMOG-1, but less than 10% in rhMOG-2 (Supplementary Fig. 2B). Thus, the batch of rhMOG-1 not only contained a wider variety of contaminating proteins, but these were also more abundant in relative amount across a large range of molecular weights (Fig. 2A). We next assessed if rhMOG-1 and rhMOG-2 had variable ability to stimulate pro-inflammatory signaling pathways.

Innate immune receptor signaling cascades induced by rhMOG batches

To assess the presence of pathogen-associated molecular pattern molecules (PAMPs) in the rhMOG-1 and rhMOG-2 preparations, we

performed bioassays for TLR2, 4, 5, and NOD2. HEK293 cells were transfected with an NF- κ B dependent reporter gene (luciferase), and with individual innate immune receptors. Activation of these receptors was assessed by measuring the expression of luciferase in response to PAMP activation by specific ligands. The rhMOG-2 preparation did not significantly stimulate luciferase expression in either of the systems used, even at the highest doses. Instead, the rhMOG-1 preparation induced a dose-dependent response via TLR2 and TLR4. Indeed, a significant increase of luciferase activity was detected for both TLR at a dose of rhMOG-1 of 2 μ g/ml as compared to 0.2 μ g/ml (TLR2, $p = 0.0002$ and TLR4, $p < 0.0001$). Moreover, the same increase was observed when comparing luciferase levels induced by rhMOG-1 as compared to rhMOG-2 at a dose of 2 μ g/ml (TLR2 and TLR4, $p < 0.0001$) and 20 μ g/ml (TLR2, $p = 0.0065$ and TLR4, $p = 0.0020$) (Fig. 2B, C). In addition, rhMOG-1, but not rhMOG-2, significantly enhanced NF- κ B dependent luciferase expression in the THP-1 bioassay at the highest dose of 20 μ g/ml of rhMOG-1 as compared to 2 μ g/ml of rhMOG-1 ($p = 0.0004$) or of 20 μ g/ml of rhMOG-2 ($p = 0.0015$). By contrast, neither rhMOG-1 nor rhMOG-2 induced NF- κ B-dependent luciferase expression via TLR5 or NOD2 (Supplementary Fig. 3). These results indicate that the rhMOG-1 preparation contains bacterial contaminants with the ability to trigger innate immune responses via TLR2 and TLR4, whereas such contaminants were not detected in the rhMOG-2 preparation.

Histopathology of the brain lesions

Most lesions from all macaques with clinical EAE ($n = 18$) were submitted to histologic evaluation. These animals presented different types of lesions, including active and prephagocytic lesions as well as areas of normal-appearing white matter (NAWM). Most of the animals harbored more than one lesion type. All brains and spinal cord lesions were classified according to their most important histologic features in one of four lesion types (Table 1).

Active lesions. Active lesions could be further subdivided into two subtypes according to their histologic characteristics and localization. This included confluent demyelination (lesion type 1) and perivascular mononuclear infiltration (lesion type 2).

Confluent demyelination (lesion type 1): Lesions with confluent demyelination were observed in the cortical white matter (CWM), profound WM (PWW), medulla (MED), and cerebellar WM (CBLWM). This lesion type was most frequent in the CWM compared to other anatomic locations. In addition, the number of lesions observed at these locations was higher in MOG1

immunized group compared to the MOG2 group (*CVM*: MOG1: 11 lesions in 6/10 animals, MOG2: 2 lesions in 2/8 animals; *PWM*: MOG1: 4 lesions in 3/10 animals, MOG2: 2 lesions in 2/8 animals; *MED*: MOG1: 3 lesions in 3/10 animals, MOG2: 1 lesion in 1/8 animals; *CBLWM*: MOG1: 3 lesions, 3/10 animals, MOG2: no lesions).

Histologically, two main features characterized this lesion type, including large confluent demyelination and infiltration with macrophages and neutrophils (Fig. 3A). Demyelinated areas were composed of multiple confluent areas of myelin destruction, which often surrounded a central venule. The myelin in these areas was completely disrupted and phagocytized by infiltrating microglia/macrophages and neutrophils. Hemorrhages, neuropil necrosis, and prominent reactive astrocytosis were further hallmarks of this lesion type, which were mainly seen in animals immunized with MOG1. The axonal injury was observed in animals immunized with both MOG types and seen especially in necrotic parts of the lesion, as evidenced by the presence of axonal swelling. Pronounced inflammation represented the second key feature of this lesion type. Central venules were surrounded by a prominent perivascular infiltrate, mainly composed of microglia/macrophages, neutrophils, and fewer CD3⁺ lymphocytes (Fig. 3E, I). The involved neuropil was highly infiltrated by myelin-laden microglia/macrophages and neutrophils with centrifugal distribution around central vessels.

The distribution of immunoglobulins (i.e., IgG) and complement (i.e., C1q) were evaluated in addition to the profile of inflammatory cells (Fig. 3M, Q). Both proteins were seen especially in the cytoplasm of myelin-laden macrophages colocalized with phagocytized myelin debris, highlighted through its LFB and MBP positivity. In addition, IgG and C1q proteins often covered residual intact myelin fibers inside the lesion, and they were seen on the intact myelin fibers in the vicinity of the lesion with no association to infiltrating macrophages. These lesion parts were interpreted as perilesional NAWM.

The perivascular mononuclear infiltration (lesion type 2): The perivascular lesions were seen at a relative distance of larger active phagocytic lesions and rarely as alone standing lesions. This lesion type was more frequent in animals immunized with MOG2 (*CWM*: MOG1: 1 lesion in 1/10 animals, MOG2: no lesions; *PWM*: MOG1: 1 lesion in 1/10 animals, MOG2: 4 lesions in 4/8 animals; *MED*: MOG1: no lesions, MOG2: 1 lesion in 1/10 animals; *CBLWM*: MOG1: 1 lesion in 1/10 animals; MOG2: no lesions).

Histologically perivascular lesions were characterized by moderate perivascular infiltration by microglia/macrophages and lymphocytes and by activation of microglia and astrocytes as highlighted by a relative increase of Iba1 and GFAP labeling (Fig. 3B, F, J). Myelin-laden macrophages and myelin vacuolation were nearly absent in this lesion type and there were relatively few perivascular and infiltrating CD3 positive lymphocytes.

A relatively low quantity of IgG and C1q proteins were present in the intact white matter surrounding activated vessels and were mainly associated with normal-appearing myelin (Fig. 3N, R).

Prephagocytic lesions. Lesions with myelin vacuolation and minimal cellular infiltrate were interpreted as prephagocytic lesions (lesion type 3) and were mainly seen in the periphery of active phagocytic lesions and less frequently without any visible connection to another lesion. This lesion type was more frequently observed in *CWM* of MOG1 immunized animals (*CWM*: MOG1: 3 lesions in 3/10 animals, MOG2: 1 lesion in 1/8 animals; *PWM and MED*: MOG1 and MOG2: no lesions; *CBLWM*: MOG1: 1 lesion in 1/10 animals, MOG2: no lesions).

The main key feature of this lesion type is myelin vacuolation (myelin edema) with relatively few infiltrating phagocytic cells (Fig. 3C). Intralésional vessels showed no or few infiltrating cells, identified as microglia/macrophages by the Iba1 marker. This lesion type showed a high diffuse upregulation of microglial/

macrophagic and astrocytic markers in the neuropil, whereas there were virtually no CD3 positive cells (Fig. 3G, K).

IgG and C1q proteins were present in a high relative quantity and were mainly associated with vacuolated myelin and cells with oligodendrocytes, astroglial and microglial appearance (Fig. 3O, S).

Normal appearing white matter. Areas with morphologically normal-appearing white matter and with upregulation of microglial and/or astrocytic markers (lesion type 4) were mainly seen in the vicinity of larger active lesions and rarely as alone standing lesions. The alone standing lesions were observed in *PWM* and medulla of MOG2 immunized animals, whereas this lesion type was not seen in the MOG1 group (*CWM*: MOG1 and MOG2: no lesions, *PWM*: MOG1: no lesions, MOG2: 3 lesions in 3/8 animals; *MED*: MOG1: no lesions, MOG2: 1 lesion in 1/8 animals; *CBLWM*: MOG1 and MOG2: no lesions).

The main characteristic of this lesion type is the relative absence of visible lesions observed in HE stains, including no notifiable cellular, infiltrate and no visible myelin changes (Fig. 3D). The upregulation of microglial and astrocytic markers is the second key feature of this lesion type (Fig. 3H, L). These activated microglia/macrophages and astrocytes were mainly seen surrounding of venules in *CWM* and *MED* and rarely in further surrounding neuropil. In addition, there were rare focal subependymal areas of NAWM containing a mild activation of microglia/macrophages whereas no astrocytic activation or cell infiltration was seen.

IgG showed a diffuse high expression in concerned regions whereas C1q was mainly present in the vicinity of vessels. Both proteins were associated with normal-appearing or minimally vacuolated myelin and to a lesser extent with cells with the oligodendrocyte, astrocyte, or microglia morphology (Fig. 3P, T). Furthermore, IgG and C1q proteins were regularly observed on the surface of intact ependymal cells in the immediate vicinity of the areas with microglial/macrophagic activation. In one case of the focal loss of ependymal cells, IgG and C1q were present on the resting ependymal cells and on the underlying vacuolated and normal-appearing myelin in the place where ependymal cells were lacking, indicating a possible trans-ependymal way of spreading of myelin-specific IgG.

Histopathology of the lesions of the spinal cord

Spinal cord lesions were observed in the WM of cervical and lumbar segments in 6/18 animals, including 3/10 MOG1 and 3/8 MOG2 immunized macaques. Confluent demyelinating lesions (MOG1: 2/10; MOG2: 1/8) were the most frequently observed lesions. Histologically, these lesions were characterized by intermediate to the large size of myelin destruction and by marked infiltration with myelin-laden microglia/macrophages. In addition, they showed marked up-regulation of the GFAP astrocytic marker and low numbers of infiltrating CD3⁺ lymphocytes (Supplementary Fig. 4A–D). One animal (MOG1 immunization) presented extended hemorrhages and mild neutrophilic infiltrates. Overlying meninges were often infiltrated with a moderate number of microglia/macrophages and with CD3⁺ lymphocytes. C1q protein was present at a moderate quantity predominantly in the phagocytic vacuoles of activated microglia/macrophages as well as in the infiltrating cells and extracellular compartment of meninges. IgG immunoglobulins were absent in these lesions except in the meninges (Supplementary Fig. 4E–F).

The perivascular lesions were seen in two animals with MOG2 immunization, whereas no such lesions were recorded in MOG1 animals. As described for the brain, these spinal cord lesions were characterized by oligofocal perivascular infiltrates with microglia/macrophages and CD3⁺ lymphocytes as well as by a mild up-regulation of GFAP and Iba1 markers next to the injured vessels with no myelin vacuolation or phagocytosis in the surrounding neuropil. These lesions were accompanied by minimal quantities

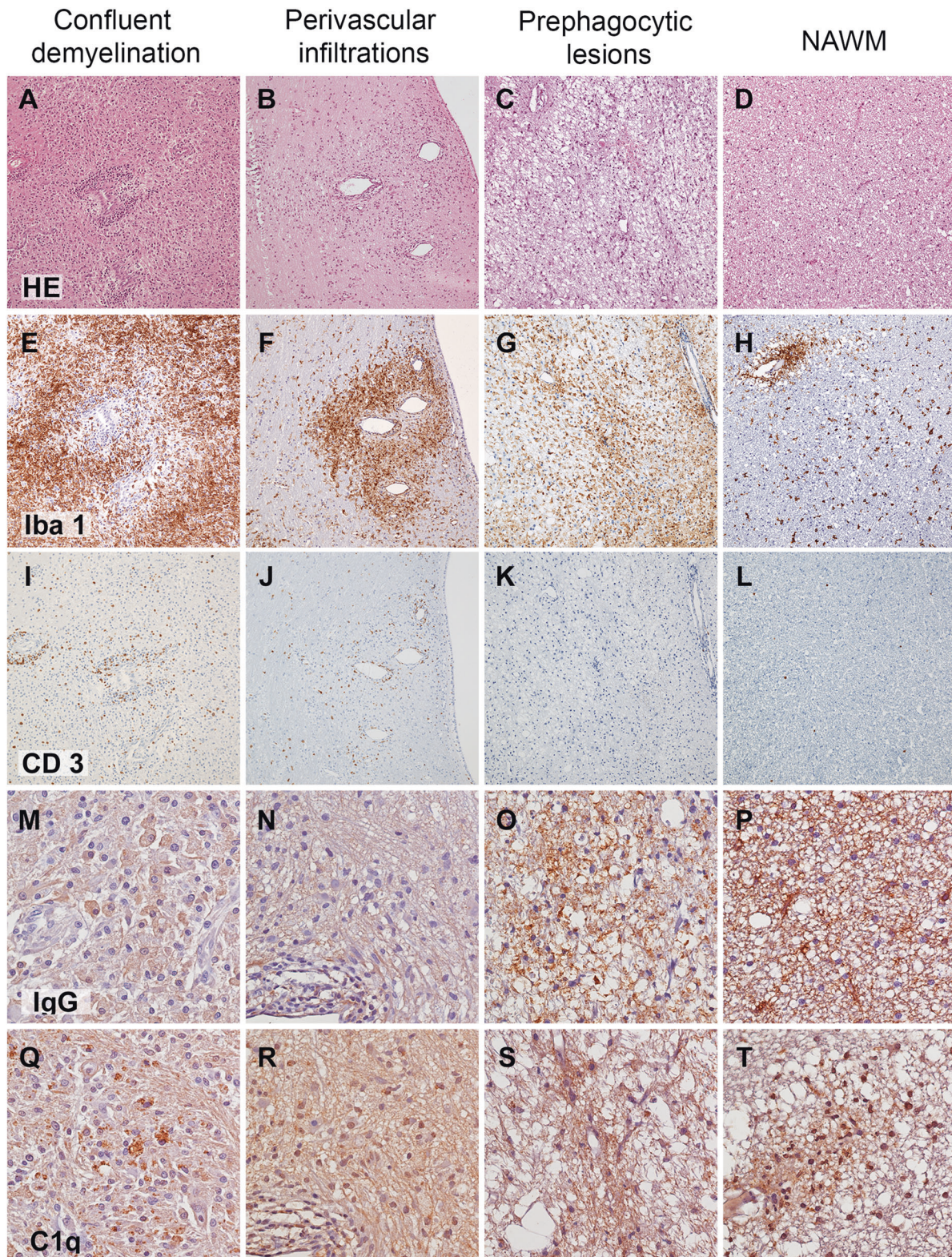


Fig. 3 Histopathologic characteristics of observed brain lesions types. **A–D** HE stains. **E–H** Iba-1 microglia/macrophagic marker expression. **I–L** CD3 expression in T lymphocytes. **M–P** IgG deposits. **Q–T** C1q complement protein expression. Note a relatively high number of infiltrating microglia/macrophages and CD3 positive lymphocytes in the confluent demyelination and perivascular infiltration lesion types and a relatively low IgG and C1q expression in these lesion types. In contrast to this, prephagocytic lesion and NAWM present an upregulation of Iba-1 intensity, no notifiable cellular infiltrate, and relatively high IgG and C1q expression. **A–L** 100× magnification. **M–T** 200× magnification.

of IgG and C1q proteins presented exclusively in the perivascular spaces.

In addition to the above-named lesion types, one prephagocytic lesion was observed in the subpial white matter of one MOG1 immunized animal. It was characterized by moderate myelin vacuolation and moderate activation of microglia/macrophages and astrocytes and rare CD3+ perivascular lymphocytes. For technical reasons, IgG and C1q proteins could not be visualized in this animal.

Comparison of the severity of the brain and spinal cord lesions

To compare the overall severity of one lesion, we created a cumulative severity score (Table 1). This score was based on a sum of the severity scores for individual histologic changes (i.e., hemorrhage, myelin vacuolation, neuropil necrosis, macrophagic, neutrophilic, and lymphocytic infiltration). Obtained scale grades for each observed lesion scored between 0 and 27. As the next step, a mean cumulative severity score per animal was built by creating an average of severity grades for all lesions in each animal. Obtained mean cumulative severity score was used for comparisons between the group MOG1 and MOG2.

There was a significant difference ($p < 0.02$) in overall severity between MOG1 and MOG2 immunized animals (Fig. 1E). Indeed, in the brain, the mean cumulative severity score of MOG1 immunized macaques (13.5 ± 4) was significantly higher than that of animals receiving MOG2 immunization (7.9 ± 5). A similar tendency could be observed concerning the spinal cord lesions. However, the difference between both groups was not significant (MOG1: mean cumulative severity score 10.7 ± 2.5 ; MOG2: mean cumulative severity score 5.7 ± 2.9), ($p = 0.08$).

DISCUSSION

In this study, we show that two rhMOG/IFA emulsions prepared with rhMOG of separate origins and disparate purity, elicit variable intensity of immune activation and cause EAE of different severity in macaques. The rhMOG with the highest level of *E. coli* contaminants induced increased innate immune receptor signaling and produced a more severe EAE than the purer rhMOG, which favored a milder and more progressive disease. Thus, the differences in immune activation and in the clinical and histologic appearance of EAE could be attributed to contaminants from the *E. coli* expression system in which the rhMOG protein was produced. Clinically, the milder EAE observed in the MOG2 group was defined by a decreased mean severity grade and an increased number of remissions, reflecting longer disease development time. Histologically, a significant decrease in overall lesion severity and a higher number of early lesions (i.e., NAWM and prephagocytic lesions) were also observed in the MOG2 immunization group. In addition, animals immunized with rhMOG-2 displayed subacute lesions, including lower frequency and severity of hemorrhage, necrosis, and neutrophil infiltration. These clinical and histopathologic characteristics reflect more closely demyelinating lesions commonly observed in human ADD. Indeed, mononuclear infiltrates of different severity are frequently observed in acute active plaques in multiple sclerosis (MS), in acute disseminated encephalomyelitis (ADEM), and in neuromyelitis optica (NMO), whereas neuropil necrosis, hemorrhages, and marked neutrophilic infiltration is observed with low frequency in these diseases. However, the last three hallmarks are observed in rare forms of demyelinating diseases, including the Marburg variant of MS, the hyperacute variant of ADEM (Hurst syndrome), and in severe lesions of NMO¹. Taken together, the lower severity and subacute character of histologic lesions resemble more closely to the lesions observed in ADD. Thus, such an improved model of EAE, induced with the purest rhMOG, can be better used for understanding the pathophysiology of autoimmune

demyelination. Especially the study of NAWM and of the prephagocytic lesions could give valuable insights into the pathogenesis of initiation of demyelination. In this model of a more progressive EAE, the observed initial prephagocytic lesions are characterized by low visible changes in HE stains, including variable myelin vacuolation and virtually no cellular infiltrate. On the other hand, these lesions often show marked microglial activation and deposits of IgG and complement (C1q) on the myelin. These characteristics are very similar to the observations made in the pattern II lesions of MS¹. Antibody-mediated demyelinated lesions are found in other MOG-sensitized EAE models, including mouse and NHP models²⁷. Myelin destruction is induced by the cooperation between encephalitogenic T cells, demyelinating anti-MOG antibodies, and complement activation²⁸.

The specific target of these complement-activating antibodies has not yet been identified, despite the facts that elevated immunoglobulins and activated complement components are present in the CSF of MS patients, that serum and CSF from patients with MS can cause demyelination in animals, and that immunoglobulin deposition and complement activation are present in immune pattern II lesions^{28,29}.

In this study, we show that bacterial contamination, hardly detectable with common techniques such as electrophoresis, may increase the severity of EAE in NHP, by playing a role of an additional adjuvant. Several mechanisms are important in the ability of adjuvants to enhance immune responses and Toll-like receptors (TLR) are one of the most important ways to activate innate immunity. These TLR, also known as pattern recognition receptors, are expressed by antigen-presenting cells and bind to components from microorganisms that lead to activation of antigen-presenting cells³⁰. Activation of TLR by bacterial components either deliberately administered or inadvertently present in immunizing mixtures has been referred to as the immunologist's "dirty little secret"³¹. The first identified and most extensively studied TLR in mammals is TLR4, which is the receptor that mediates effects by lipopolysaccharide (LPS), the endotoxin secreted by Gram-negative bacteria³². We found TLR4 ligands in MOG1 emulsion, which could stimulate this recognition pathway in vivo and contribute to the aggravation of EAE. As described previously, an anterior BPRC rhMOG preparation showed only a slight stimulation of TLR4 (± 2.4 -fold increase) by the highest rhMOG concentration in transfected HEK239 cells and it was not clear if traces of LPS could elicit an immune-stimulating effect in vivo²⁰. Experiments in laboratory rodents have shown that LPS alone is not sufficient for EAE development as it may induce production of IL-10 by dendritic cells and because TLR4 knockout does not prevent EAE³³. In addition, LPS treatment prior to or during the induction phase of EAE significantly delayed the onset of disease^{34,35}. On the other hand, Saul et al. showed that LPS-matured bone marrow-derived dendritic cells could initiate autoimmune pathology in mice³⁶. Furthermore, high concentrations of LPS may induce TLR 4 hyperstimulation inducing transient impairment of T cell trafficking to the CNS due to altered chemokine gradients³⁵. Taken together these studies suggest that LPS alone represents an insufficient stimulus to initiate EAE in rodents, but it can contribute to the development of lesions. Thus, the effective EAE development depends in this case on the time and degree of stimulation. Bacterial peptidoglycan (PGN) is a further important component of the wall of Gram-positive and Gram-negative bacteria, which could amplify autoimmune pathology via activation of innate immune cells³⁷. Indeed, PGN or its fragments activate pattern recognition receptors including TLR2, NOD-like receptors (NLR), and specialized PGN recognition proteins (PGLYRP1–4)³⁸. We observed increased activation of TLR2 pathway by MOG1 compared to MOG2, however, found bacterial residuals did not activate NLR in the present study. It appears that bacterial PGN fragments could favor EAE induction

and replace mycobacterial wall fragments in mouse EAE is driven by the MOG35-55 peptide. Furthermore, antibodies directed against the Muramyl dipeptide, a signature motif of PGN, limit mouse EAE, indicating that endogenous PGN contributes to brain inflammation^{37,38}.

Our observations strongly suggest that a minimal quantity of bacterial proteins associated with rhMOG can increase the severity of EAE in non-human primates. Even if the mature immune system of NHP does not necessarily need “danger” signals to reactivate encephalitogenic T and B cells and initiate EAE, the severity of clinical signs and histologic lesions could be enhanced through these additional “danger” signals as shown in marmosets³⁹. Moreover, systemic LPS injection initiates a wide range of inflammatory responses in the brain, including an increase of cytokines, chemokines, prostaglandins, and nitric oxide⁴⁰. In addition, LPS can also disrupt the integrity of the blood-brain barrier, leading to its increased permeability for anti-myelin antibodies and autoimmune T and B cells^{32,41}.

As stressed in materials and methods, the main limitation of this study is that the two cohorts of macaques were immunized in two different facilities. This implies that factors inherent to either laboratory and different from the purity of rhMOG may have contributed to modulating the course of EAE. Future experiments of EAE induction in cynomolgus macaques with rhMOG of controlled purity shall confirm that this sole precaution allows inducing the more progressive model of EAE in macaques with all the characteristics described in the present work.

In conclusion, here we describe that a milder form of EAE can be obtained in macaques. We propose that low levels of contamination of rhMOG with bacterial proteins are sufficient to increase the severity of clinical and histologic hallmarks of EAE in the cynomolgus macaque. The obtained refined EAE model with milder histologic lesions reflects more accurately human demyelinating diseases and allows studying the pathogenesis of disease initiation.

AVAILABILITY OF DATA AND MATERIAL

The data supporting the conclusions of this article are included within the article. Original slides, tissues, and photographs are retained. All reagents and animals used in this study are available from scientific supply companies, which depending on supply, may be available upon request.

REFERENCES

- Popescu, B. F. Gh & Lucchinetti, C. F. Pathology of demyelinating diseases. *Annu Rev Pathol Mech Dis* **7**, 185–217 (2012).
- Peiris, M., Monteith, G. R., Roberts-Thomson, S. J. & Cabot, P. J. A model of experimental autoimmune encephalomyelitis (EAE) in C57BL/6 mice for the characterisation of intervention therapies. *J Neurosci Methods* **163**, 245–254 (2007).
- Behan, P. O. & Chaudhuri, A. EAE is not a useful model for demyelinating disease. *Mult Scler Relat Disord* **3**, 565–574 (2014).
- Namer, I. J. et al. The role of Mycobacterium tuberculosis in experimental allergic encephalomyelitis. *Eur Neurol* **34**, 224–227 (1994).
- Hasselmann, J. P. C., Karim, H., Khalaj, A. J., Ghosh, S. & Tiwari-Woodruff, S. K. Consistent induction of chronic experimental autoimmune encephalomyelitis in C57BL/6 mice for the longitudinal study of pathology and repair. *J Neurosci Methods* **284**, 71–84 (2017).
- Felix, N. J. et al. Targeting lymphocyte co-stimulation: from bench to bedside. *Autoimmunity* **43**, 514–525 (2010).
- Sedlacek, H. H., Wanger, R. & Bengelsdorff, H. J. Influence of various immunomodulators on the induction of experimental autoimmune encephalomyelitis in Lewis rats. *Immunobiology* **157**, 99–108 (1980).
- Stosic-Grujicic, S., Ramic, Z., Bumbasirevic, V., Harhaji, L. & Mostarica-Stojkovic, M. Induction of experimental autoimmune encephalomyelitis in Dark Agouti rats without adjuvant. *Clin Exp Immunol* **136**, 49–55 (2004).
- Segal, B. M., Klinman, D. M. & Shevach, E. M. Microbial products induce autoimmune disease by an IL-12-dependent pathway. *J Immunol* **158**, 5087–5090 (1997).
- Segal, B. M., Chang, J. T. & Shevach, E. M. CpG oligonucleotides are potent adjuvants for the activation of autoreactive encephalitogenic T cells in vivo. *J Immunol* **164**, 5683–5688 (2000).
- Nagai, Y. et al. Minimum structural requirements for encephalitogen and for adjuvant in the induction of experimental allergic encephalomyelitis. *Cell Immunol* **35**, 158–167 (1978).
- Linthicum, D. S. & Frelinger, J. A. Acute autoimmune encephalomyelitis in mice. II. Susceptibility is controlled by the combination of H-2 and histamine sensitization genes. *J Exp Med* **156**, 31–40 (1982).
- Munoz, J. J., Bernard, C. C. & Mackay, I. R. Elicitation of experimental allergic encephalomyelitis (EAE) in mice with the aid of pertussigen. *Cell Immunol* **83**, 92–100 (1984).
- Mostarica-Stojković, M., Vukmanović, S., Petrović, M., Ramić, Z. & Lukić, M. L. Dissection of adjuvant and suppressive effects of mycobacteria in experimental allergic encephalomyelitis production. *Int Arch Allergy Appl Immunol* **85**, 82–86 (1988).
- Tsunoda, I., Kuang, L. Q., Theil, D. J. & Fujinami, R. S. Antibody association with a novel model for primary progressive multiple sclerosis: induction of relapsing-remitting and progressive forms of EAE in H2s mouse strains. *Brain Pathol* **10**, 402–418 (2000).
- Andreasen, C., Powell, D. A. & Carbonetti, N. H. Pertussis toxin stimulates IL-17 production in response to Bordetella pertussis infection in mice. *PLoS ONE* **4**, e7079 (2009).
- Stimmer, L., Fovet, C.-M. & Serguera, C. Experimental models of autoimmune demyelinating diseases in nonhuman primates. *Vet Pathol* **55**, 27–41 (2018).
- Dunham, J. et al. Blockade of CD127 exerts a dichotomous clinical effect in marmoset experimental autoimmune encephalomyelitis. *J Neuroimmune Pharmacol* **11**, 73–83 (2016).
- Hart, B. A., van Kooyk, Y., Geurts, J. J. G. & Gran, B. The primate autoimmune encephalomyelitis model; a bridge between mouse and man. *Ann Clin Transl Neurol* **2**, 581–593 (2015). t.
- Haanstra, K. G. et al. Induction of experimental autoimmune encephalomyelitis with recombinant human myelin oligodendrocyte glycoprotein in incomplete Freund's adjuvant in three non-human primate species. *J Neuroimmune Pharmacol* **8**, 1251–1264 (2013).
- Regen, T. & Waisman, A. Modeling a complex disease: multiple sclerosis-update 2020. *Advances in Immunology* **149**, 25–34 (2021).
- Jagessar, S. A. et al. Induction of progressive demyelinating autoimmune encephalomyelitis in common marmoset monkeys using MOG34-56 peptide in incomplete freund adjuvant. *J Neuropathol Exp Neurol* **69**, 372–385 (2010).
- Hartmann, E. M., Allain, F., Gaillard, J.-C., Pible, O. & Armengaud, J. Taking the shortcut for high-throughput shotgun proteomic analysis of bacteria. *Methods Mol Biol* **1197**, 275–285 (2014).
- Klein, G. et al. RNA-binding proteins are a major target of silica nanoparticles in cell extracts. *Nanotoxicology* **10**, 1555–1564 (2016).
- Christie-Oleza, J. A., Fernandez, B., Nogales, B., Bosch, R. & Armengaud, J. Proteomic insights into the lifestyle of an environmentally relevant marine bacterium. *ISME J* **6**, 124–135 (2012).
- Serguera, C. et al. Anti-MOG autoantibodies pathogenicity in children and macaques demyelinating diseases. *J Neuroinflamm* **16**, 244 (2019).
- Mayer, M. C. & Meinel, E. Glycoproteins as targets of autoantibodies in CNS inflammation: MOG and more. *Ther Adv Neurol Disord* **5**, 147–159 (2012).
- Peschl, P. et al. Human antibodies against the myelin oligodendrocyte glycoprotein can cause complement-dependent demyelination. *J Neuroinflamm* **14**, 208 (2017).
- Lucchinetti, C. et al. Heterogeneity of multiple sclerosis lesions: implications for the pathogenesis of demyelination. *Ann Neurol* **47**, 707–717 (2000).
- Kigerl, K. A., de Rivero Vaccari, J. P., Dietrich, W. D., Popovich, P. G. & Keane, R. W. Pattern recognition receptors and central nervous system repair. *Exp Neurol* **258**, 5–16 (2014).
- Janeway, C. A. Pillars article: approaching the asymptote? Evolution and revolution in immunology. *Cold Spring Harb Symp Quant Biol.* **54**, 1–13. *J Immunol* **191**, 4475–4487 (2013).
- Mallard, C. Innate immune regulation by toll-like receptors in the brain. *ISRN Neurol* **2012**, 701950 (2012).
- Zhou, H. et al. Differential IL-10 production by DCs determines the distinct adjuvant effects of LPS and PTX in EAE induction. *Eur J Immunol* **44**, 1352–1362 (2014).
- Buenafe, A. C. & Bourdette, D. N. Lipopolysaccharide pretreatment modulates the disease course in experimental autoimmune encephalomyelitis. *J Neuroimmunol* **182**, 32–40 (2007).
- O'Brien, K. et al. Role of the innate immune system in autoimmune inflammatory demyelination. *Curr Med Chem* **15**, 1105–1115 (2008).
- Saul, L., Besusso, D. & Mellanby, R. J. LPS-matured CD11c+ bone marrow-derived dendritic cells can initiate autoimmune pathology with minimal injection site inflammation. *Lab Anim* **51**, 292–300 (2017).
- Laman, J. D., 't Hart, B. A., Power, C. & Dziarski, R. Bacterial peptidoglycan as a driver of chronic brain inflammation. *Trends Mol Med* **26**, 670–682 (2020).
- Visser, L. et al. Proinflammatory bacterial peptidoglycan as a cofactor for the development of central nervous system autoimmune disease. *J Immunol* **174**, 808–816 (2005).

39. Jagessar, S. A., Dijkman, K., Dunham, J., Hart, B.t.A. & Kap, Y. S. Experimental autoimmune encephalomyelitis in marmosets. *Methods Mol Biol* **1304**, 171–186 (2016).
40. Erickson, M. A. & Banks, W. A. Cytokine and chemokine responses in serum and brain after single and repeated injections of lipopolysaccharide: multiplex quantification with path analysis. *Brain Behav Immunol* **25**, 1637–1648 (2011).
41. Stolp, H. B. et al. Breakdown of the blood-brain barrier to proteins in white matter of the developing brain following systemic inflammation. *Cell Tissue Res* **320**, 369–378 (2005).

ACKNOWLEDGEMENTS

We thank Philippe Hantraye for reagents and discussion.

AUTHOR CONTRIBUTIONS

CMF, CS, HC, JA, JB, JC, LS, PH: contributed to the acquisition and analysis of data. CMF, JC, JM, LS: Animal's follow-up, samples collection, and MRI. AJ, EA, GM, JV, EA, PH: laboratory dosages. AP, LS, JC, HC: tissue treatments and histology. CMF, CS, HC, JA, JB, JC, LS: graphs and statistical analysis. B'tH, CS, HC, JA, JB, JC, KD, LS, PhH, RLG: manuscript drafting for main intellectual content. AJ, AP, BA, CMF, CS, EA, GM, HC, JA, JB, JC, JM, JV, KD, LS, PH, RLG gave final approval to the article.

FUNDING

Infrastructures Nationales en Biologie et Santé (INBS)—2011 Infectious Disease Models and Innovative Therapies (IDMIT), ANR-11-INBS-0008. INSERM, CNRS—Délégation Régionale Midi-Pyrénées Limousin, Cynbiose, ANR-11-RPIB-0005.

COMPETING INTERESTS

The authors declare no competing interests.

ETHICS APPROVAL AND CONSENT TO PARTICIPATE

Following European directive 2010/63/UE and French regulations, the project at MIRCen was performed in an agreed user establishment (agreement number C 92-032-02), with institutional permission obtained from the French Ministry of Agriculture after evaluation by an ethical committee (2015081710528804vl). At Cynbiose (agreement number N°C 69 127 0505), the project was approved by the ethical committee of VetAgro Sup (2016072117544328) under file number 1417v2. All procedures were performed in compliance with CEA's and Cynbioses's animal welfare structure under veterinary care at all times.

ADDITIONAL INFORMATION

Supplementary information The online version contains supplementary material available at <https://doi.org/10.1038/s41374-021-00646-x>.

Correspondence and requests for materials should be addressed to L.S.

Reprints and permission information is available at <http://www.nature.com/reprints>

Publisher's note Springer Nature remains neutral with regard to jurisdictional claims in published maps and institutional affiliations.